Physics Letters B 843 (2023) 138021

Contents lists available at ScienceDirect

Physics Letters B

journal homepage: www.elsevier.com/locate/physletb

Systematic study of prescission neutron multiplicity: Revealing the role of entrance channel magicity

K. Chakraborty [a,*], M.T. Senthil Kannan [b,c], Jhilam Sadhukhan [b,c], S. Mandal [a,**]

[a] Department of Physics and Astrophysics, University of Delhi, New Delhi, 110007, India
[b] Physics Group, Variable Energy Cyclotron Centre, Kolkata, 700064, India
[c] Homi Bhabha National Institute, Anushakti Nagar, Mumbai, 400094, India

ARTICLE INFO

Article history:
Received 24 March 2023
Received in revised form 18 May 2023
Accepted 9 June 2023
Available online 14 June 2023
Editor: D.F. Geesaman

Keywords:
Nuclear fission
Entrance channel shell effect
Neutron multiplicity
Statistical model calculation

ABSTRACT

The prescission neutron multiplicities (ν_{pre}) are studied for a systematic understanding of the influence of entrance-channel shell closure in fusion-fission dynamics. The existing ν_{pre} data are analyzed for reactions with a wide variety of target and projectile combinations. For completeness, the measured ν_{pre} data for the fusion-fission reactions with the doubly closed shell ^{16}O projectile on the targets having either proton (^{204,206}Pb) or both proton and neutron (^{208}Pb) shell closure is reanalyzed. Although the measured ν_{pre} for ^{224}Th disagree with the available data reported by Rossner et al. (1992) [1], our results are found to be more consistent and follow a systematic trend as described in this letter. Theoretical analysis is performed within the standard statistical model framework, where dissipation strength is used as a tunable parameter. It is observed that irrespective of the compound nuclear excitation energy, the entrance channel magicity imparts an intriguing impact on the dissipation strength. A similar entrance channel effect in the evaporation residue cross-section is also demonstrated. In conclusion, the present analysis establishes an entanglement of the exit channel observables with the entrance channel shell closure. It contradicts the hypothesis of complete equilibrium in compound nuclear reactions.

1. Introduction

Comprehending the fission dynamics of an excited compound nucleus (CN) is unaccomplished without embracing the dissipative nature of collective nuclear motion. Dissipation controls the energy loss mechanism of fission (collective) degrees of freedom and delays the journey of a CN across the fission barrier, thus manifesting a reduced flux across the barrier [2], an increased saddle to scission time [3], and an enhanced particle emission during the decay process [4]. Therefore, dissipative models of fission decay [5,6] are conventionally employed to explain the measured prescission neutron multiplicity (ν_{pre}). In addition, shell corrections are important around the closed shell compound nuclei [7]. For example, it has been shown that appropriate shell corrections must be incorporated in order to correctly predict the dissipation strength from the measured ν_{pre} [7]. Apart from these, the collective enhancement in the nuclear level density [8] and the orientation of the compound nuclear spin [8,9] may also impact fission dynamics.

The above-mentioned static and dynamical corrections are usually implemented with the fate that an equilibrated CN is formed after fusion, and therefore, the separate identities of the target and projectile are completely lost. Hence, although the influence of entrance-channel magicity and isospin are investigated [10] in the quasi-fission process, such effects are hardly considered in fission dynamics. Neutrons evaporated during the formation of a CN may contribute to ν_{pre}. However, studies along this direction [11,12] are limited.

In spite of ample measurements and continued efforts [4,12–15], understanding the global systematic of ν_{pre} and its implication to the fusion-fission dynamics is still incomplete. It gives us the opportunity to explore the role of the entrance channel shell structure in ν_{pre} and subsequently, in the magnitude of dissipation strength estimated within the conventional statistical model calculations. The ν_{pre} from various experiments [1,4,7,12,16–23] are considered in the present study with a restriction on the projectile mass to avoid any contribution from non-compound decay channels. Further, with the same motivation, we measured ν_{pre} in the fission of three different even-even isotopes of Th: ^{220,222,224}Th. Particularly, we chose the doubly magic projectile ^{16}O with the magic ^{204,206}Pb and doubly magic ^{208}Pb as targets. The ν_{pre} for the ^{16}O + ^{208}Pb reaction was already measured in a previous

* Principal Corresponding author.
** Corresponding author.
E-mail addresses: kajolchakraborty.du@gmail.com (K. Chakraborty), smandal@physics.du.ac.in (S. Mandal).

https://doi.org/10.1016/j.physletb.2023.138021

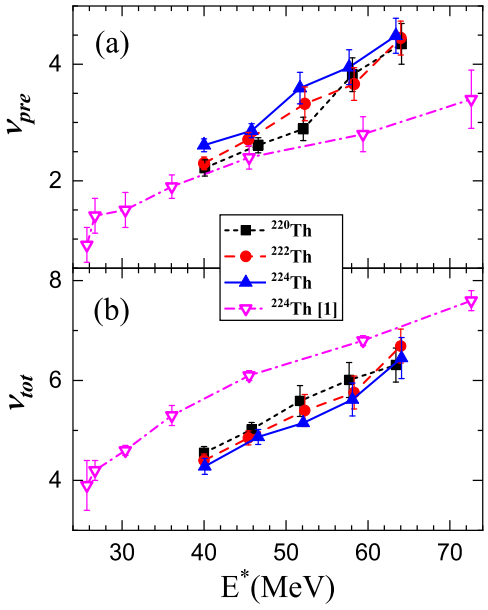

Fig. 1. (a) Variation of ν_{pre} and (b) ν_{tot} as a function of excitation energy E^* for the present measurement (filled symbols) and from [1] (open symbols).

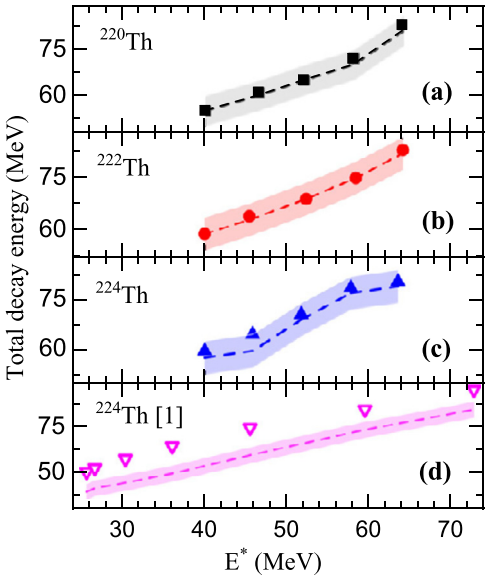

Fig. 2. Total available decay energy ($E_x(f)$) as a function of E^* for the present measurement (filled symbols) and from [1] (open symbols), calculated using Eq. (1) (dashed lines) and Eq. (2) (symbols). Errors in $E_x(f)$ are shorter than the height of the symbols. The colour bands represent a spread of ±5 MeV (see text).

experiment [1] and these ν_{pre} are often used to benchmark theoretical models [6,24,25]. Although our results disagree with the previous measurement, current values obey the energy balance criterion [16]. Interestingly, as described below, the present results follow a systematic trend in contrast to the existing data.

The Letter is organized as follows. The neutron multiplicity measurement and its disagreement with the earlier results [1] are justified in Sec. 2. The rationale for reviewing the ν_{pre} data within the bounds of target and projectile magicity is discussed in Sec. 3. The statistical model framework employed to analyze the data and the systematic analysis of the results are performed in Sec. 4. Finally, we summarize in Sec. 5.

2. Neutron multiplicity measurement

Neutron multiplicities for the ^{16}O + ^{204,206,208}Pb reactions have been measured by using the National Array of Neutron Detectors facility at the Inter University Accelerator Centre (IUAC), New Delhi, India. Pulsed ^{16}O beam (repetition rate = 250 ns, beam width ≈1 ns) was accelerated to lab energies of 90 to 120 MeV using the 15 UD Pelletron + Superconducting Linear Accelerator (LINAC) and bombarded on the self-supporting isotopically enriched ^{204,206,208}Pb targets of thickness ≈1.5 mg/cm^2. Two position-sensitive Multi Wire Proportional Counters (MWPCs) of area 20×10 cm^2 were placed symmetrically at distances of 19.6 cm and 21 cm and at angles (θ_{lab}, ϕ_{lab}) of (70^0, 90^0) and (-80^0, 270^0) with respect to the forward beam direction. 16 (12.7×12.7 cm^2) NE213 organic liquid scintillators were kept at a flight path of 200 cm from the target in the reaction plane for neutron detection. Further details of the experimental set-up can be found elsewhere [26]. The data is analyzed using the software framework of ROOT [27]. The efficiency of neutron detectors is calculated by using the Monte-Carlo-based multi-particle transport code FLUKA [28]. The solid angle and efficiency corrected double-differential neutron energy spectra of all the 16 detectors are fitted simultaneously to extract the prescission (ν_{pre}) and post-scission components (ν_{post}) of neutron multiplicity. The three-moving-source (one CN and two fission fragments) least square fitting procedure is employed to isolate ν_{pre} from ν_{post} as per the detailed procedure described in [29]. Fig. 1 shows ν_{pre} and the total neutron multiplicity ν_{tot} ($= \nu_{pre} + 2\nu_{post}$) for the present measurements and also compares these for ^{224}Th with the previous measurement in [1]. The present ν_{pre} (ν_{tot}) values for ^{224}Th are consistently higher (lower) in the entire excitation energy (E^*) range. This mismatch between the two measurements is scrutinized by estimating the total available fission-decay energy $E_x(f)$ from ν_{tot}. The part of $E_x(f)$ responsible for particle evaporation is [16]

$$E_x(f) = E_{\text{c.m.}} + Q(f) - E_k, \tag{1}$$

where $E_{\text{c.m.}}$ is the centre-of-mass energy for the reaction and E_k is the kinetic energy of the fission fragments governed by the Viola systematic [30]. The $Q(f)$ is the Q-value of the fission reaction and, assuming symmetric fission, it can be obtained from the target's mass M_T, projectile's mass M_P, and fission fragments' mass M_f as $Q(f) = M_P + M_T - 2M_f$. If we assume that $E_x(f)$ is completely utilized by neutron and γ-ray emissions (other light particles like the proton and α can be neglected for the present purpose) then [16],

$$E_x(f) = E_\gamma(f) + \nu_{tot}\,(8.07 + E_n), \tag{2}$$

where $E_\gamma(f)$ is the total excitation energy carried away by γ-ray emissions, 8.07 is the mass defect of a neutron in MeV, and E_n is the average kinetic energy carried away by each emitted neutron. For ^{224}Th, $E_\gamma(f)$ has been estimated using the γ-emission spectra for ^{208}Pb (^{16}O, f) reaction [31]. Considering similar γ-emission probabilities for ^{220,222,224}Th, the $E_\gamma(f)$ for ^{220,222}Th are assumed to be same as ^{224}Th for similar values of E^*. The mismatch in $E_x(f)$ obtained from Eq. (1) and from Eq. (2) could be ±5 MeV [16] and, as shown in Fig. 2(a-c), our results fall within this limit. Therefore, it validates the consistency of present ν_{pre} data. However, for the values reported in [1], there is a minimum of 10% difference between the two $E_x(f)$ values as shown in Fig. 2(d). Specifically, a larger $E_x(f)$ from Eq. (2) indicates an overestimation of ν_{tot}. Therefore, a lower ν_{tot} would have been more desirable from the previous measurement. Since ν_{pre} and ν_{tot} are correlated,

Table 1
Details of the reactions selected in the present work. The δ_{sh} is defined in the text.

S.No	CN	Reaction	δ_{sh}	Ref.	S.No	CN	Reaction	δ_{sh}	Ref.
1	^{197}Tl	^{16}O+^{181}Ta	-27	[19]	15	^{216}Rn	^{18}O+^{198}Pt	-8	[21]
2	^{197}Tl	^{19}F+^{178}Hf	-27	[19]	16	^{216}Ra	^{12}C+^{204}Pb	-8	[22] [33]^{a}
3	^{200}Pb	^{19}F+^{181}Ta	-24	[16] [34,35]^{a}	17	^{216}Ra	^{19}F+^{197}Au	-8	[22] [33]^{a}
4	^{203}Bi	^{19}F+^{184}W	-21	[18] [36]^{a}	18	^{217}Fr	^{19}F+^{198}Pt	-7	[7]
5	^{204}Pb	^{18}O+^{186}W	-20	[20]	19	^{220}Th	^{16}O+^{204}Pb	-4	[*] [37]^{a}
6	^{206}Po	^{12}C+^{194}Pt	-18	[17]	20	^{222}Th	^{16}O+^{206}Pb	-2	[*]
7	^{210}Po	^{12}C+^{198}Pt	-14	[17] [38,39]^{a}	21	^{224}Th	^{16}O+^{208}Pb	0	[*] [1] [40,41]^{a}
8	^{210}Po	^{18}O+^{192}Os	-14	[16] [34]^{a}	22	^{228}U	^{19}F+^{209}Bi	+4	[23]
9	^{210}Rn	^{16}O+^{194}Pt	-14	[21] [42]^{a}	23	^{229}Np	^{20}Ne+^{209}Bi	+5	[4]
10	^{212}Rn	^{18}O+^{194}Pt	-12	[21] [43]^{a}	24	^{243}Am	^{11}B+^{232}Th	+19	[12]
11	^{213}Fr	^{19}F+^{194}Pt	-11	[7] [44]^{a}	25	^{244}Cm	^{12}C+^{232}Th	+20	[12]
12	^{213}Fr	^{16}O+^{197}Au	-11	[16] [40]^{a}	26	^{248}Cf	^{11}B+^{237}Np	+24	[12]
13	^{214}Rn	^{16}O+^{198}Pt	-10	[21]	27	^{248}Cf	^{16}O+^{232}Th	+24	[12]
14	^{215}Fr	^{19}F+^{196}Pt	-9	[7]	28	^{251}Es	^{19}F+^{232}Th	+27	[16]

[*] Present measurement of ν_{pre}.
[a] Ref. for evaporation residue cross-section.

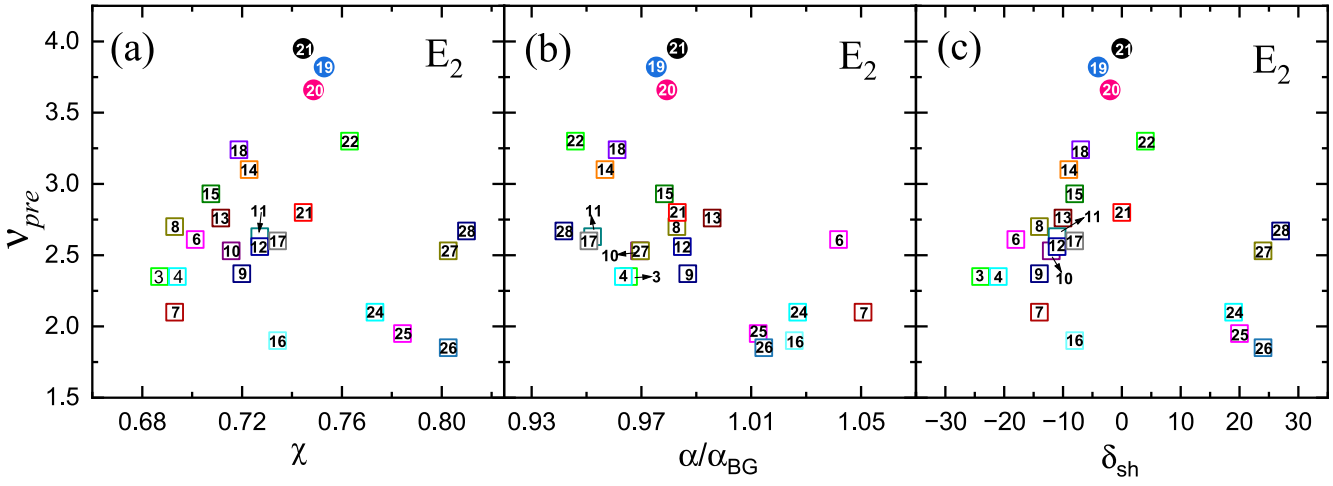

Fig. 3. Variation of available (open squares) and measured (filled circles) ν_{pre} in the energy group E_2 along (a) the fissility parameter χ; (b) the ratio α/α_{BG}; and (c) the deviation δ_{sh} (see text for definition). The errors in ν_{pre} lie within the height of the symbols. Numerical values in each symbol identify the serial number in Table 1.

a detailed reanalysis is required to rule out any inconsistency in the ν_{pre} data of [1].

3. Systematics of prescission neutron multiplicity

We compare the available (including present measurements) ν_{pre} data of 28 reactions in the compound nuclear mass range of $197 \leq M_{CN} \leq 251$. Details of the reactions are given in Table 1. Non-compound processes like quasi-fission become prevalent for reactions with $M_P > 20$ [32]. Therefore, we choose reactions with $M_P \leq 20$ to avoid contamination from such processes. All the data are grouped into three different E^* bins to minimize any dependence on the excitation energy. These bins are defined as E_1: 45 MeV $\leq E^* \leq$ 55 MeV, E_2: 55 MeV $\leq E^* \leq$ 65 MeV, and E_3: 65 MeV $\leq E^* \leq$ 75 MeV. Although ν_{pre} data also exists for $E^* > 80$ MeV, the general conclusion from the present work does not depend on the absolute magnitude of E^*. Also, for a few reactions, there are multiple data points within the energy window of 10 MeV. Since ν_{pre} does not vary much within this energy range, we just pick a single point.

To explore the entrance channel dependence of fusion-fission reactions, two different global parameters can be selected, (i) the ratio of the entrance channel mass asymmetry $\alpha = (|M_T - M_P|)/(M_T + M_P)$ with the Businaro-Gallone critical mass asymmetry α_{BG} [45], *i.e.* α/α_{BG}, and (ii) the deviation δ_{sh} of the neutron and proton numbers in the target and projectile from the respective nearest magic numbers. For the chosen reactions, it is apparent that ^{16}O and ^{208}Pb are the doubly shell-closed reference nuclei to measure δ_{sh} of the projectile and target, respectively. For example, in the case of ^{12}C + ^{204}Pb reaction, $(\delta_{sh})_{\text{proj,neut}} = N_{^{12}\text{C}} - N_{^{16}\text{O}} = 6 - 8 = -2$, similarly $(\delta_{sh})_{\text{proj,prot}} = Z_{^{12}\text{C}} - Z_{^{16}\text{O}} = -2$, $(\delta_{sh})_{\text{tar,neut}} = N_{^{204}\text{Pb}} - N_{^{208}\text{Pb}} = -4$, and $(\delta_{sh})_{\text{tar,prot}} = Z_{^{204}\text{Pb}} - Z_{^{208}\text{Pb}} = 0$. Adding all four contributions, we get $\delta_{sh} = -8$. Hence, δ_{sh} is a cumulative measure of the deviation from the magicity of a given target-projectile combination. Here, instead of using the absolute values of deviations, we preserve the sign for each term since particle excess from the magic number may have different effects compared to a deficiency of the same magnitude. In respect to this newly defined parameter δ_{sh}, our present measurements are crucial as the corresponding δ_{sh}s (-4, -2, 0) fill the gap around $\delta_{sh} = 0$. For completeness, we also consider the fissility χ of the CN [46] as an additional global parameter.

At first, we consider the excitation energy bin E_2 where data for most of the reactions in Table 1 are available. The variation of ν_{pre} with χ is shown in Fig. 3(a). Fission hindrance usually decreases with increasing χ and, therefore, a monotonic reduction in ν_{pre} with χ was expected. However, within the covered range of χ, a broad distribution of ν_{pre} can be observed in Fig. 3(a). A faint peak-like structure develops with large ν_{pre} near $\delta_{sh} = 0$, but

this behaviour can not be correlated with the variation of χ. In Fig. 3(b), we demonstrate the distribution of ν_{pre} along α/α_{BG}. The ratio α/α_{BG} determines the direction of mass flow among the target and projectile and the corresponding formation delay of the CN. For $\alpha/\alpha_{BG} > 1$, the light projectile is absorbed within the heavy target, which usually occurs at a faster speed than the mass equilibration in a more symmetric reaction with $\alpha/\alpha_{BG} \lesssim 1$ [12]. Since formation delay results in an enhanced ν_{pre}, we expect ν_{pre} to decrease with α/α_{BG}. Interestingly, such a trend can be observed in Fig. 3(b) indicating the presence of an entrance-channel effect in ν_{pre}. Nevertheless, present results deviate from the observed trend. It may be because of strong shell corrections in the target and projectile ($\delta_{sh} \approx 0$) that surpass the effects driven by α/α_{BG}. However, more data points with different values of α/α_{BG} but $\delta_{sh} \approx 0$ are required to confirm this speculation.

Finally, inspired by previous outcomes [4,10,12,13], a fair conjecture is made to investigate the effect of entrance channel shell structure on ν_{pre}. Fig. 3(c) shows the variation of ν_{pre} with δ_{sh} for the energy group E_2. A systematic behaviour with a maximum at $\delta_{sh} = 0$ and a nearly symmetric sharp fall on either side is quite visible. Although, the older ν_{pre} data [1] for ^{224}Th lies out of the systematic pattern along with a few other data points. Fig. 3(c) hints toward a considerable impact of entrance channel magicity on the neutron emission mechanism. There is a scarcity of data in the $\delta_{sh} > 0$ region, where more measurements should be performed.

4. Statistical model analysis

To establish the above observation on firm ground, we perform a statistical model analysis of all the reactions in Table 1 by using the Monte-Carlo-method based code VECSTAT [8]. A brief explanation of the main ingredients of the model is given below. For the steady-state fission probability, it uses the Kramers' fission width [47],

$$\Gamma_f = \frac{\hbar\omega_{gs}}{T}\Gamma_{BW}\left(\sqrt{1+\left(\frac{\beta}{2\omega_s}\right)^2} - \frac{\beta}{2\omega_s}\right), \tag{3}$$

where T is the nuclear temperature, ω_{gs} and ω_s are the best-fit harmonic oscillator frequencies [48] that mimic the potential energy profile around the ground state and saddle configurations respectively, and β is the reduced dissipation strength. Here, β is a tunable parameter adjusted to reproduce the experimental ν_{pre}. The Bohr-Wheeler fission width Γ_{BW} can be written as [47,49],

$$\Gamma_{BW} = \frac{1}{2\pi\rho(E^*)}\int_0^{E^*-V_B} \rho(E^* - V_B - \epsilon)d\epsilon, \tag{4}$$

where ρ [50] is the density of states at the respective configurations and V_B is the angular-momentum dependent fission barrier height, calculated from the finite-range liquid drop model [51]. V_B is further modified with the deformation-dependent shell corrections [52]. The Γ_f in Eq. (3) is corrected for the orientation of the compound nuclear spin [53,54]. The initial transient part of the fission width is parameterized by using the standard exponential growth [55].

The ρ in Eq. (4) is calculated from the Fermi gas model [50], where the analytic form of ρ depends on the nuclear level density parameter a, which is further written in terms of temperature as $T = \sqrt{E^*/a}$. We adopt the deformation dependent a [57] which is further corrected for shell effects as suggested by Ignatyuk [58]. In addition, collective enhancement in the level density [53] is incorporated. The decay widths for the emission of light particles

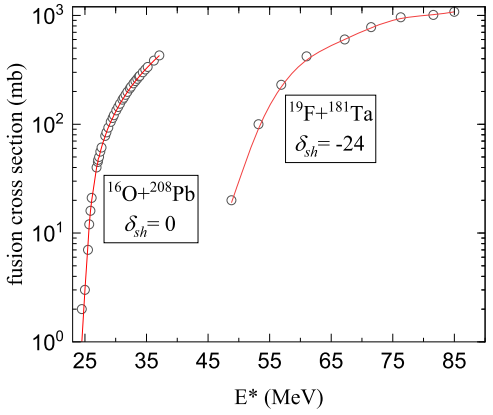

Fig. 4. Calculated fusion cross sections (solid lines) are compared with experimental values (symbols) for ^{16}O + ^{208}Pb [56] and ^{19}F + ^{181}Ta [34].

(neutron, proton, and α) and GDR γ-ray are estimated from the Weisskopf formula as given in [6]. Multiple Monte Carlo samplings are performed to decide the faith of each event in an ensemble of compound nuclei.

Within the formalism of compound nuclear decay, the fusion spin distribution or equivalently the compound nuclear spin distribution directly connects the entrance channel properties with the post-equilibrium dynamics. Specifically, the magicity of target and/or projectile nuclei suppose to populate lower spin due to their shape compactness. Therefore, once the fusion spin distribution is precisely known, it apparently takes care of all the entrance channel effects and the parameters like β, responsible for the subsequent dynamics, are expected to be independent of the entrance channel properties. It is therefore essential to estimate the fusion spin distribution very accurately. To this end, we use the parametrization prescribed in [6] because it predicts the correct fusion spin distributions for light projectiles [59]. To assess the accuracy of our spin distributions, we compare the corresponding fusion cross-sections with the measured values. It is demonstrated in Fig. 4 for two different reactions with extreme values of δ_{sh}. Evidently, the experimental fusion cross-sections are well reproduced. Hence, the entrance channel dependence of the compound nuclear spin distribution is properly taken care of, and further explanation for the observed δ_{sh} dependence of ν_{pre} can not be attributed to any miscalculation of compound nuclear spin.

To isolate the relevance of entrance channel shell effects, the identification of possible interference with the compound nuclear shell structure is essential. To this end, two different sets of calculations are performed: in Set-I, no shell corrections are included in V_B and a as well and, in Set-II, all the compound nuclear shell corrections are considered. The β values obtained for the Set-I calculations are shown in Fig. 5 as a function of δ_{sh}. It can be seen that β replicates the same trend as observed for ν_{pre}: a maximum at $\delta_{sh} = 0$ and decreases symmetrically on either side. Further, this variation of β is independent of the compound nuclear excitation energy, i.e. almost the same for all the three excitation energy bins. Particularly, in E_3, β is well-correlated to δ_{sh} apart from a few exceptions including the ν_{pre} of ^{224}Th from [1]. Concerning this older measurement, the mismatch in ν_{pre} (Fig. 1(a)) from our results is more prominent at higher E^*. As a result, the deviation of the corresponding β from the systematics is more for E_2 and E_3 compared to E_1.

The Set-I exhibits a strong excitation energy dependence of β. Consequently, the required magnitudes of β for E_1, E_2, and E_3 are quite different as shown in Fig. 5. This is in contrast to the generic behaviour of one-body dissipation, which is believed to be independent of excitation energy [60]. The dependence of β on excitation energy is noticeably reduced in the second set (Set-II)

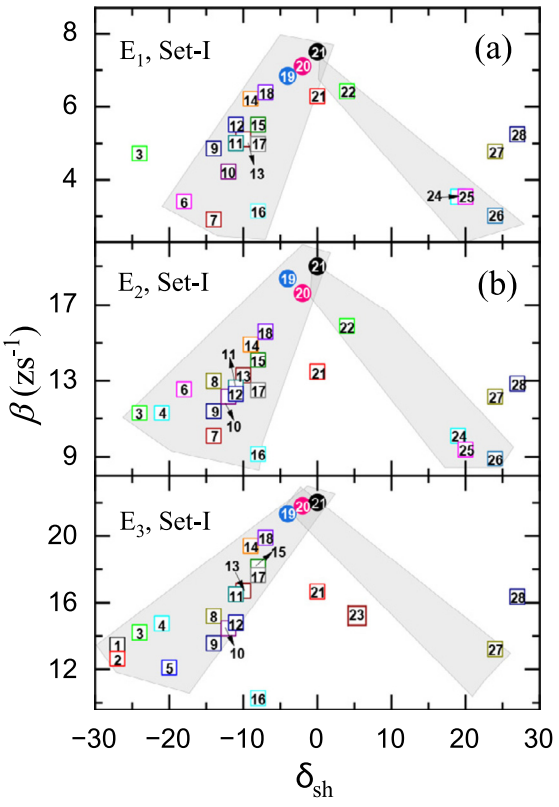

Fig. 5. Variation of the reduced dissipation coefficient β with δ_{sh} obtained for Set-I in the excitation energy bin (a) E_1, (b) E_2, and (c) E_3 (see text for definitions). Symbols have the same meaning as in Fig. 3. Shaded regions are drawn to guide the eyes.

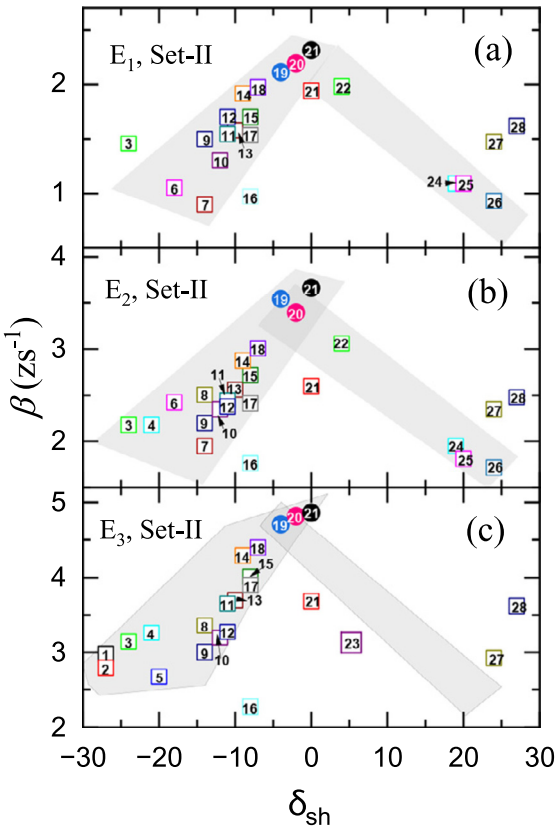

Fig. 6. Same as Fig. 5 calculated with shell corrections (Set-II).

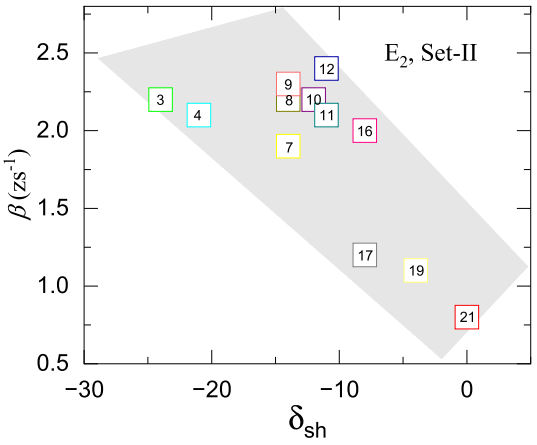

Fig. 7. Variation of β with δ_{sh} obtained by fitting the ER cross-section data. Symbols have the same meaning as in Fig. 3.

of calculation where shell corrections are incorporated. The extracted β for Set-II are illustrated in Fig. 6. It shows that β for E_1, E_2, and E_3 are of similar magnitude. Apart from this difference, the general pattern of β along δ_{sh} is almost identical to that obtained for Set-I. The persistence of the same behaviour of β confirms that such dependence on the entrance channel magicity is independent of the compound nuclear shell structure and other finer details of the modelling. For a more explicit understanding of the entrance channel effects, one needs to somehow include the parameters dependent on the entrance channel in the fission model. This is beyond the scope of present-day statistical model calculations for fission. The stochastic dynamical framework [6] is an obvious choice to accommodate non-equilibrium evolution as expected during the entrance channel dynamics. Although an attempt [11] has been made in this direction, more realistic calculations are required.

Another aspect of fusion-fission dynamics, explored in the present work, is the independent role of the target-projectile mass asymmetry α. To accomplish this goal, we select particular reactions from Table 1 where the same CN is populated with similar E^* via different target-projectile combinations. Five pairs of such reactions are {1, 2} (^{197}Tl), {7, 8} (^{210}Po), {11, 12} (^{213}Fr), {16, 17} (^{216}Ra), and {26, 27} (^{248}Cf) with αs equal to {0.84, 0.81}, {0.89, 0.83}, {0.82, 0.85}, {0.89, 0.82}, and {0.91, 0.87}, respectively. In each pair, δ_{sh} is equal for both reactions. Hence, δ_{sh} can not be responsible for the observed differences in ν_{pre} (Fig. 3(c)) and the associated β (Fig. 6). Interestingly, the mismatch in β (and ν_{pre} as well) within each pair is somehow correlated to the corresponding difference in α, *i.e.* δ_α. Evidently, βs within a pair are close to each other for {1, 2} and {11, 12} where $\delta_\alpha = 0.03$. In contrast, the βs are quite distinct for {7, 8}, {16, 17} and {26, 27} where $\delta_\alpha \geq 0.04$. Also, for these pairs, a stronger dissipation strength is required to reproduce ν_{pre} for the more symmetric (lower α) reaction. It indicates the possibility of pre-equilibrium neutron emission as the pre-equilibrium time or the formation delay is more for the comparatively symmetric reaction. However, direct experimental and theoretical evidence of such a phenomenon is still missing. We can conclude that, apart from δ_{sh}, α also influences the neutron emission process in fusion-fission reactions.

A shape-dependent β with a higher value in the post-saddle region is deemed essential to simultaneously fit the ν_{pre} and ER cross-sections [24]. However, the motivation behind the present work is to understand the role of entrance channel parameters in fission, which is supposedly independent of the exact nature of dissipation during the post-equilibrium dynamics. Therefore, instead of using any shape dependence, we readjust β to simulate

the experimental ER cross-sections for 12 reactions in Table 1 for the E_2 bin. The absolute values of these newly evaluated β may not be useful as they do not simultaneously reproduce the measured ν_{pre}, but, in the context of the present work, this simple strategy is extremely effective in investigating the entrance channel dependence in ER cross-section. The extracted βs are plotted in Fig. 7 as a function of δ_{sh}. We could study only the $\delta_{sh} < 0$ reactions due to the lack of available data for positive δ_{sh} in this excitation energy window. It can be seen that, in general, slightly lower values of β are required to fit the ER cross-section. This is anticipated as the ER cross-section is essentially governed by the dynamics in the pre-saddle region where dissipative forces are expected to be small due to shape compactness [61]. Fig. 7 demonstrates a systematic dependence of β on δ_{sh}: minimum β is required for $\delta_{sh} = 0$ and then it gradually increases as δ_{sh} deviates from zero. A careful comparison between Fig. 6(b) and Fig. 7 reveals that the required β for both ν_{pre} and ER cross-section almost saturates within a narrow band of $2\ \mathrm{zs}^{-1} \lesssim \beta \lesssim 2.5\ \mathrm{zs}^{-1}$ in the case of $|\delta_{sh}| \gtrsim 10$. This signifies the disappearance of the sensitivity to the entrance channel magicity at such large deviations from the magic numbers. We should add here that the β in Fig. 6(c) also shows such inertness to δ_{sh}. The most peculiar behaviour of β is that it manifests an inverse dependency on δ_{sh} for ν_{pre} compared to ER cross-section. Whereas large β is required for ν_{pre} near the doubly magic target and projectile, it tends to decrease for ER cross-section at the same δ_{sh}. It also predicts that, for magic and near magic targets and projectiles, a stronger shape dependence in β is necessary to simultaneously reproduce the experimental ν_{pre} and ER cross-section *viz-a-viz* the fission cross-section. An appropriate theoretical framework is yet to be developed to resolve the intricacies of the contrasting nature of β for the two fission observables. Although initiatives [8,24,53] have been taken within the concepts of compound nuclear decay, the present observation demands the incorporation of pre-equilibrium dynamics even when the compound system reaches a complete equilibration before it decays.

5. Summary

A systematic analysis of available ν_{pre} and ER cross-section data is performed. Further, the measured neutron multiplicities for ^{16}O + ^{204,206,208}Pb reactions are revisited to complete the analysis. We observed strong dependence of fission observables on the entrance channel magicity. Also, the connection with the entrance channel mass asymmetry is discussed. Detailed statistical model calculations suggest the presence of entrance channel effects in the extracted dissipation strength. Our analysis reveals an urgency for developing comprehensive dynamical modelling that accounts for all dynamical correlations and finer structural details like the shell effects in colliding nuclei starting from the collision stage. Subsequently, more measurements of neutron multiplicity with ^{16}O or a nearby projectile and heavy targets between ^{208}Pb and ^{232}Th are required to get further correlation in the present study.

Declaration of competing interest

The authors declare that they have no known competing financial interests or personal relationships that could have appeared to influence the work reported in this paper.

Data availability

Data will be made available on request.

Acknowledgements

KC is thankful to Dr. Savi Goyal (PhD Supervisor: SM) for providing the details of the experiment with ^{16}O beam performed as part of latter's PhD thesis work. KC and SM duly acknowledge all personnel at IUAC involved in the successful execution of the experiment with ^{16}O beam. Useful discussions with Dr. Santanu Pal are acknowledged.

References

[1] H. Rossner, D. Hinde, J. Leigh, J. Lestone, J. Newton, J. Wei, S. Elfström, Phys. Rev. C 45 (1992) 719.
[2] P. Grangé, H. Weidenmüller, Phys. Lett. B 96 (1980) 26–30.
[3] D. Hilscher, H. Rossner, B. Cramer, B. Gebauer, U. Jahnke, M. Lehmann, E. Schwinn, M. Wilpert, T. Wilpert, H. Frobeen, E. Mordhorst, W. Scobel, Phys. Rev. Lett. 62 (1989) 1099–1102.
[4] D.J. Hinde, H. Ogata, M. Tanaka, T. Shimoda, N. Takahashi, A. Shinohara, S. Wakamatsu, K. Katori, H. Okamura, Phys. Rev. C 39 (1989) 2268–2284.
[5] H.A. Kramers, Physica 7 (1940) 284–304.
[6] P. Fröbrich, I. Gontchar, Phys. Rep. 292 (1998) 131–237.
[7] V. Singh, B.R. Behera, M. Kaur, A. Kumar, P. Sugathan, K.S. Golda, A. Jhingan, M.B. Chatterjee, R.K. Bhowmik, D. Siwal, S. Goyal, J. Sadhukhan, S. Pal, A. Saxena, S. Santra, S. Kailas, Phys. Rev. C 87 (2013) 064601.
[8] T. Banerjee, S. Nath, S. Pal, Phys. Lett. B 776 (2018) 163–167.
[9] J.P. Lestone, Phys. Rev. C 59 (1999) 1540–1544.
[10] C. Simenel, D. Hinde, R. du Rietz, M. Dasgupta, M. Evers, C. Lin, D. Luong, A. Wakhle, Phys. Lett. B 710 (2012) 607–611.
[11] N. Kumar, S. Verma, S. Mohsina, J. Sadhukhan, K.R. Devi, A. Banerjee, N. Saneesh, M. Kumar, R. Mahajan, M. Thakur, G. Kaur, A. Rani Neelam, A. Yadav Kavita, R. Kumar Unnati, S. Mandal, S. Kumar, B. Behera, K. Golda, A. Jhingan, P. Sugathan, Phys. Lett. B 814 (2021) 136062.
[12] A. Saxena, A. Chatterjee, R.K. Choudhury, S.S. Kapoor, D.M. Nadkarni, Phys. Rev. C 49 (1994) 932–940.
[13] M. Itkis, A.Y. Rusanov, Phys. Part. Nucl. 29 (1998) 160–200.
[14] C. Schmitt, A. Lemasson, K.-H. Schmidt, A. Jhingan, S. Biswas, Y.H. Kim, D. Ramos, A.N. Andreyev, D. Curien, M. Ciemala, E. Clément, O. Dorvaux, B. De Canditiis, F. Didierjean, G. Duchêne, J. Dudouet, J. Frankland, B. Jacquot, C. Raison, D. Ralet, B.-M. Retailleau, L. Stuttgé, I. Tsekhanovich, Phys. Rev. Lett. 126 (2021) 132502.
[15] K. Mahata, C. Schmitt, S. Gupta, A. Shrivastava, G. Scamps, K.-H. Schmidt, Phys. Lett. B 825 (2022) 136859.
[16] D. Hinde, R. Charity, G. Foote, J. Leigh, J. Newton, S. Ogaza, A. Chattejee, Nucl. Phys. A 452 (1986) 550–572.
[17] K. Golda, A. Saxena, V. Mittal, K. Mahata, P. Sugathan, A. Jhingan, V. Singh, R. Sandal, S. Goyal, J. Gehlot, A. Dhal, B. Behera, R. Bhowmik, S. Kailas, Nucl. Phys. A 913 (2013) 157–169.
[18] I. Mukul, S. Nath, K.S. Golda, A. Jhingan, J. Gehlot, E. Prasad, S. Kalkal, M.B. Naik, T. Banerjee, T. Varughese, P. Sugathan, N. Madhavan, S. Pal, Phys. Rev. C 92 (2015) 054606.
[19] H. Singh, A. Kumar, B.R. Behera, I.M. Govil, K.S. Golda, P. Kumar, A. Jhingan, R.P. Singh, P. Sugathan, M.B. Chatterjee, S.K. Datta Ranjeet, S. Pal, G. Viesti, Phys. Rev. C 76 (2007) 044610.
[20] N.K. Rai, A. Gandhi, A. Kumar, N. Saneesh, M. Kumar, G. Kaur, A. Parihari, D. Arora, K.S. Golda, A. Jhingan, P. Sugathan, T.K. Ghosh, J. Sadhukhan, B.K. Nayak, N.K. Deb, S. Biswas, A. Chakraborty, Phys. Rev. C 100 (2019) 014614.
[21] R. Sandal, B.R. Behera, V. Singh, M. Kaur, A. Kumar, G. Singh, K.P. Singh, P. Sugathan, A. Jhingan, K.S. Golda, M.B. Chatterjee, R.K. Bhowmik, S. Kalkal, D. Siwal, S. Goyal, S. Mandal, E. Prasad, K. Mahata, A. Saxena, J. Sadhukhan, S. Pal, Phys. Rev. C 87 (2013) 014604.
[22] H. Singh, K.S. Golda, S. Pal Ranjeet, R. Sandal, B.R. Behera, G. Singh, A. Jhingan, R.P. Singh, P. Sugathan, M.B. Chatterjee, S.K. Datta, A. Kumar, G. Viesti, I.M. Govil, Phys. Rev. C 78 (2008) 024609.
[23] H. Singh, B.R. Behera, G. Singh, I.M. Govil, K.S. Golda, A. Jhingan, R.P. Singh, P. Sugathan, M.B. Chatterjee, S.K. Datta, S. Pal, Ranjeet, S. Mandal, P.D. Shidling, G. Viesti, Phys. Rev. C 80 (2009) 064615.
[24] J. Sadhukhan, S. Pal, Phys. Rev. C 81 (2010) 031602.
[25] P.N. Nadtochy, E.G. Ryabov, A.E. Gegechkori, Y.A. Anischenko, G.D. Adeev, Phys. Rev. C 85 (2012) 064619.
[26] S. Goyal, S. Mandal, A. Jhingan, P. Sugathan, S. Pal, B. Behera, K. Golda, H. Singh, S. Kalkal, V. Singh, R. Garg, D. Siwal, M. Kaur, M. Saxena, S. Kumar, S. Verma, M. Gupta, S. Roy, R. Singh, in: EPJ Web of Conferences, in: EDP Sciences, vol. 86, 2015, 00013.
[27] R. Brun, F. Rademakers, Nucl. Instrum. Methods Phys. Res., Sect. A, Accel. Spectrom. Detect. Assoc. Equip. 389 (1997) 81–86.
[28] A. Ferrari, P. Sala, A. Fasso, J. Ranft, Technical Report, CERN-2005-10, INFN/TC 05/11, SLAC, 2005, https://www.slac.stanford.edu/pubs/slacreports/reports16/slac-r-773.pdf.

[29] D. Hilscher, J.R. Birkelund, A.D. Hoover, W.U. Schröder, W.W. Wilcke, J.R. Huizenga, A.C. Mignerey, K.L. Wolf, H.F. Breuer, V.E. Viola, Phys. Rev. C 20 (1979) 576–591.
[30] V.E. Viola, K. Kwiatkowski, M. Walker, Phys. Rev. C 31 (1985) 1550–1552.
[31] M. Thoennessen, D. Chakrabarty, M. Herman, R. Butsch, P. Paul, Phys. Rev. Lett. 59 (1987) 2860.
[32] B.B. Back, Phys. Rev. C 31 (1985) 2104–2112.
[33] A. Berriman, D. Hinde, M. Dasgupta, C. Morton, R. Butt, J. Newton, Nature 413 (2001) 144–147.
[34] R. Charity, J. Leigh, J. Bokhorst, A. Chatterjee, G. Foote, D. Hinde, J. Newton, S. Ogaza, D. Ward, Nucl. Phys. A 457 (1986) 441–460.
[35] D. Hinde, J. Leigh, J. Newton, W. Galster, S. Sie, Nucl. Phys. A 385 (1982) 109–132.
[36] S. Nath, P.V.M. Rao, S. Pal, J. Gehlot, E. Prasad, G. Mohanto, S. Kalkal, J. Sadhukhan, P.D. Shidling, K.S. Golda, A. Jhingan, N. Madhavan, S. Muralithar, A.K. Sinha, Phys. Rev. C 81 (2010) 064601.
[37] D.J. Hinde, M. Dasgupta, A. Mukherjee, Phys. Rev. Lett. 89 (2002) 282701.
[38] A. Shrivastava, S. Kailas, A. Chatterjee, A.M. Samant, A. Navin, P. Singh, B.S. Tomar, Phys. Rev. Lett. 82 (1999) 699–702.
[39] A. Shrivastava, S. Kailas, A. Chatterjee, A. Navin, A.M. Samant, P. Singh, S. Santra, K. Mahata, B.S. Tomar, G. Pollarolo, Phys. Rev. C 63 (2001) 054602.
[40] K.-T. Brinkmann, A.L. Caraley, B.J. Fineman, N. Gan, J. Velkovska, R.L. McGrath, Phys. Rev. C 50 (1994) 309–316.
[41] M.M. Hosamani, N.M. Badiger, N. Madhavan, I. Mazumdar, S. Nath, J. Gehlot, A.K. Sinha, S.M. Patel, P.B. Chavan, T. Varughese, V. Srivastava, M.M. Shaikh, P.S. Devi, P.V. Laveen, A. Shamlath, M. Shareef, S.K. Duggi, P.V.M. Rao, G.N. Jyothi, A. Tejaswi, P.N. Patil, A. Vinayak, K.K. Rajesh, A. Yadav, A. Parihari, R. Biswas, M. Dhibar, D.P. Kaur, M. Ratna Raju, J. Joseph, Phys. Rev. C 101 (2020) 014616.
[42] E. Prasad, K.M. Varier, N. Madhavan, S. Nath, J. Gehlot, S. Kalkal, J. Sadhukhan, G. Mohanto, P. Sugathan, A. Jhingan, B.R.S. Babu, T. Varughese, K.S. Golda, B.P. Ajith Kumar, B. Satheesh, S. Pal, R. Singh, A.K. Sinha, S. Kailas, Phys. Rev. C 84 (2011) 064606.
[43] E. Prasad, P. Laveen, N. Madhavan, S. Nath, J. Gehlot, K. Varier, A. Jhingan, A. Vinodkumar, A. Shamlath, B. Babu, B. Behera, R. Sandal, V. Singh, J. Sadhukhan, S. Pal, S. Kailas, in: Proceedings of the DAE Symp. on Nucl. Phys, vol. 58, 2013, p. 534.
[44] V. Singh, B.R. Behera, M. Kaur, A. Kumar, K.P. Singh, N. Madhavan, S. Nath, J. Gehlot, G. Mohanto, A. Jhingan, I. Mukul, T. Varughese, J. Sadhukhan, S. Pal, S. Goyal, A. Saxena, S. Santra, S. Kailas, Phys. Rev. C 89 (2014) 024609.
[45] U. Businaro, S. Gallone, Nuovo Cimento (1955-1965) 5 (1957) 315–317.
[46] W. Swiatecki, Nucl. Phys. A 376 (1982) 275–291.
[47] J. Sadhukhan, S. Pal, Phys. Rev. C 79 (2009) 064606.
[48] J. Sadhukhan, S. Pal, Phys. Rev. C 78 (2008) 011603.
[49] N. Bohr, J.A. Wheeler, Phys. Rev. 56 (1939) 426–450.
[50] A.N. Bohr, B.R. Mottelson, World Scientific Publishing Company, 1998.
[51] A.J. Sierk, Phys. Rev. C 33 (1986) 2039–2053.
[52] W.D. Myers, W.J. Swiatecki, Nucl. Phys. 81 (1966) 1–60.
[53] T. Banerjee, S. Nath, S. Pal, Phys. Rev. C 99 (2019) 024610.
[54] R. Kaur, M. Kaur, S. Pal, Phys. Rev. C 106 (2022) 024604.
[55] K.H. Bhatt, P. Grangé, B. Hiller, Phys. Rev. C 33 (1986) 954–968.
[56] C.R. Morton, D.J. Hinde, J.R. Leigh, J.P. Lestone, M. Dasgupta, J.C. Mein, J.O. Newton, H. Timmers, Phys. Rev. C 52 (1995) 243–251.
[57] W. Reisdorf, Z. Phys. A 300 (1981) 227–238.
[58] A. Ignatyuk, G. Smirenkin, A. Tishin, Yad. Fiz. 21 (1975) 485–490.
[59] S. Mohsina, J. Sadhukhan, Phys. Rev. C 101 (2020) 044607.
[60] J.P. Lestone, S.G. McCalla, Phys. Rev. C 79 (2009) 044611.
[61] G. Chaudhuri, S. Pal, Phys. Rev. C 65 (2002) 054612.